The Astrophysical Journal, 751:135 (9pp), 2012 June 1 doi:10.1088/0004-637X/751/2/135

H_2D^+ IN THE HIGH-MASS STAR-FORMING REGION CYGNUS X

T. Pillai[1], P. Caselli[2], J. Kauffmann[3,4], Q. Zhang[3], M. A. Thompson[5], and D. C. Lis[1]
[1] Cahill Center for Astronomy and Astrophysics, California Institute of Technology, Pasadena, CA 91125, USA; tpillai@astro.caltech.edu
[2] School of Physics and Astronomy, University of Leeds, Leeds LS2 9JT, UK
[3] Center for Astrophysics, 60 Garden Street, Cambridge, MA 02138, USA
[4] Jet Propulsion Laboratory, California Institute of Technology, 4800 Oak Grove Drive, Pasadena, CA 91109, USA
[5] Centre for Astrophysics Research, Science and Technology Research Institute, University of Hertfordshire, Herts AL10 9AB, UK
Received 2012 January 23; accepted 2012 March 30; published 2012 May 15

ABSTRACT

H_2D^+ is a primary ion that dominates the gas-phase chemistry of cold dense gas. Therefore, it is hailed as a unique tool in probing the earliest, prestellar phase of star formation. Observationally, its abundance and distribution is, however, just beginning to be understood in low-mass prestellar and cluster-forming cores. In high-mass star-forming regions, H_2D^+ has been detected only in two cores, and its spatial distribution remains unknown. Here, we present the first map of the *ortho*-H_2D^+ $J_{k^+,k^-} = 1_{1,0} \rightarrow 1_{1,1}$ and N_2H^+ 4–3 transition in the DR21 filament of Cygnus X with the James Clerk Maxwell Telescope, and N_2D^+ 3–2 and dust continuum with the Submillimeter Array. We have discovered five very extended ($\leqslant$34,000 AU diameter) weak structures in H_2D^+ in the vicinity of, but distinctly offset from, embedded protostars. More surprisingly, the H_2D^+ peak is not associated with either a dust continuum or N_2D^+ peak. We have therefore uncovered extended massive cold dense gas that was undetected with previous molecular line and dust continuum surveys of the region. This work also shows that our picture of the structure of cores is too simplistic for cluster-forming cores and needs to be refined: neither dust continuum with existing capabilities nor emission in tracers like N_2D^+ can provide a complete census of the total prestellar gas in such regions. Sensitive H_2D^+ mapping of the entire DR21 filament is likely to discover more of such cold quiescent gas reservoirs in an otherwise active high-mass star-forming region.

Key words: ISM: abundances – ISM: clouds – ISM: individual objects (Cygnus X) – ISM: molecules – ISM: structure – radio lines: ISM – stars: formation

Online-only material: color figures

1. INTRODUCTION

In their evolution toward the formation of a young stellar object, low-mass cloud cores change their density distribution until the so-called pivotal state is reached (e.g., Shu et al. 1987). This stage is considered the starting point for protostellar accretion. Thus, it is crucial to find and study objects close to the "pivotal" stage to unveil the initial conditions in the process of star formation. We believe to have found this class of objects: they are the so-called prestellar cores, characterized by central densities of $\sim 10^6$ cm^{-3}, centrally concentrated density profiles, and with clear signs of contraction in the central few thousand AU (Caselli et al. 2002a, 2002b; Crapsi et al. 2004, 2005). They stand out in having large degrees of CO freezeout and deuterium fractionation (Bacmann et al. 2003). In particular, they show strong emission in the $J_{k^+,k^-} = 1_{1,0} \rightarrow 1_{1,1}$ line of *ortho*-H_2D^+ in the case of L1544, the prototypical low-mass prestellar core (Caselli et al. 2003). In this object, the H_2D^+ line has been mapped by Vastel et al. (2006) and found to be extended over a region of $\sim$5000 AU in projected radius. An H_2D^+ survey was conducted in low-mass cores (Caselli et al. 2008) and revealed a decrease in fractional abundance of *ortho*-H_2D^+ in protostellar cores as compared to starless cores.

To reproduce the past observations toward low-mass cores, which imply abundances of H_2D^+ close to 10^{-9} with respect to H_2, one needs to have species such as CO (which destroy H_2D^+) almost completely frozen onto dust grains (e.g., Walmsley et al. 2004; Roberts et al. 2004). This can be achieved only if the dust temperature is low ($T_{\rm dust} < 20$ K) and the density is large ($n[H_2] \geqslant 10^5$ cm^{-3}). At these conditions, all species quickly condense out (with timescales $\sim 10^9$ yr $(n[H_2]/{\rm cm}^{-3})^{-1}$, leaving mainly He, H_2, and its daughter species (in particular H_3^+ and its deuterated forms, including H_2D^+) in the gas phase. Therefore, H_2D^+ observations are a unique tool to trace and study the chemistry and kinematics of the high-density nucleus of prestellar cores, the future stellar cradle.

That being said about low-mass star formation, the early phase chemistry in massive star-forming regions is still poorly understood, mainly because the study of these regions have so far focused on molecular material associated with high-mass protostellar objects (HMPOs; e.g., Beuther et al. 2002), which are actively altering gas and dust properties. Based on our wide-field (10 × 10 arcmin) census of clouds in 32 massive star-forming regions, harboring UCHII regions, we discovered a new sample of massive pre-protocluster cores. Our program is known as SCAMPS (the SCUBA Massive Pre/Protocluster core Survey; Thompson et al. 2005). Many of the sources are seen as dark patches in infrared images of the region. As a result these clumps must have dust temperatures below 30 K (as evidenced by mid-IR upper limits) and have masses of a few 100–1000 $M_\odot$. These millimeter-peak/mid-infrared absorption sources are very promising candidates for being high-mass pre-protocluster cores.

We started investigating these pre-protocluster cores in more detail by observing them in NH_3 with the Effelsberg 100 m telescope, as well as in deuterated NH_3 with the IRAM 30 m telescope (Pillai et al. 2007). On average, the derived temperatures are around 15 K compared with average temperatures toward the previously studied more evolved HMPOs (Sridharan et al. 2002) of 22 K. Finally, depletion and very large

Table 1
Continuum Sensitivity

Source	Frequency (GHz)	R.A. (J2000) J2000	Decl. (J2000) J2000	1σ noise (mJy)	Resolution (arcsec × arcsec, deg)
G81.74+0.59	230	20:39:02.97	42:25:05.301	4.0	4.2 × 3.5, −67

deuterium fractionation, $[NH_2D]/[NH_3] \sim 0.2$, are found (Pillai et al. 2007, 2011), an enhancement of $\approx 10^4$ over the cosmic D/H ratio. With gas masses of the order of a few hundred $M_\odot$, high deuteration, depletion, and cold temperatures, these sources feature many characteristics expected for massive pre-protocluster cores. Similar large values of the deuterium fraction have been found toward quiescent cores embedded in Infrared Dark Clouds (IRDCs; Chen et al. 2010; Fontani et al. 2011). However, see also other recent deuteration studies in IRDCs (Miettinen et al. 2011; Sakai et al. 2012).

With the James Clerk Maxwell Telescope and Submillimeter Array (SMA), we observed the *ortho*-$H_2D^+(1_{1,0}–1_{1,1})$, N_2D^+ 3–2, and N_2H^+ 4–3 lines toward three cores from our sample. Here, we report the detection of the *ortho*-H_2D^+ $(1_{1,0}–1_{1,1})$ line and its large-scale emission in one of the three cores (the only core where *ortho*-H_2D^+ was detected) and subsequent mapping of the deuterated region in N_2D^+ 3–2 line with SMA.

2. SOURCE SELECTION

The JCMT observations were initially targeted toward three objects from the SCAMPS survey with the brightest NH_2D detections. In total, 23.8 hr were spent on the project on the three sources. After a few hours of integration on each of the three targets, which did not result in a detection, we decided to perform deeper integration on G81.74+0.59, since we detected the brightest NH_2D line toward it in our previous IRAM 30 m survey (Pillai et al. 2007). Here, we only discuss the observations toward G81.74+0.59. The maps presented here correspond to clumps along the DR21 filament $\sim 2'$ north of the well-known DR21(OH) massive young stellar object. The DR21 filament itself is the most massive region in the entire complex. Our mapped region coincides with three bright 1.3 mm MAMBO dust continuum peaks as revealed in a large-scale survey of Cygnus X (Motte et al. 2007). For reference, this region encompasses the massive dense core N53 of Motte et al. survey (see also Bontemps et al. 2010; Csengeri et al. 2011) and FIR 1/2/3 in infrared studies of this region (Chandler et al. 1993; Kumar et al. 2007). The embedded population identified by Kumar et al. is shown as stars in Figure 1.

3. SMA AND JCMT OBSERVATIONS

JCMT N_2H^+ and H_2D^+ observations were carried out in service mode in several sessions starting from 2007 August to 2008 August with the HARP instrument on JCMT. HARP is the heterodyne multi-pixel array at JCMT equipped with 16 receptors separated by 30 arcsec with a footprint of 2 arcmin. The beam size of each receptor is $\approx 14''$. Nyquist-sampled maps were achieved using a jiggle pattern with a position switch to move to the reference. During most of our observations, 14 of the 16 receptors were working. After finding evidence of emission at the edge of our map from the initial observing session, we shifted the map center for the subsequent sessions. The pointing accuracy was on average $<3''$, and the median system temperature at the H_2D^+ frequency was 579 K. The `smurf` software provided as a part of the Starlink package was used to regrid the data, mask the bad receptors, construct three-dimensional (3D) data cubes, and co-add the scans. The data were then converted to fits and analyzed in `CLASS`.[6]

The SMA[7] N_2D^+ and continuum observations were made with all eight antennas in the most compact configuration (subcompact) in two tracks in 2008 August and September. The observations were done in track sharing mode with several sources per track. For G81.74+0.59, we had four pointings separated at less than half a (primary) beam spacing to cover the same region as the JCMT HARP footprint at 230 and 279 GHz, respectively. The 230 GHz receiver was tuned to the CO (2–1) line in the spectral band s13 of the upper sideband for the N_2D^+ observations. We used a non-uniform correlator configuration to have a higher spectral resolution of ~ 0.2 km s^{-1} for the chunks covering the N_2D^+ and CO line. The rest of the correlator was set to ~ 0.4 km s^{-1}. The data were taken under very good weather conditions (<1 mm water vapor), and the typical system temperatures were 100 K. The gain calibrator was MWC349a, $\sim 2^\circ$ away from the target position. Uranus and 3C454.3 were used as the flux and bandpass calibrator, respectively. Flux calibration is based on SMA flux monitoring of the observed planet and is estimated to be accurate to within 20%. The primary beam at 230 GHz is $\sim 51''$. The data calibration was done in `MIR`, an IDL-based calibration package, and then exported to MIRIAD and GILDAS for further data reduction which included continuum subtraction and imaging. The center of the final image of the mosaic, the 1σ rms noise level achieved in the continuum images, and the resulting synthesized beam for all observations is listed in Table 1.

4. RESULTS

4.1. H_2D^+ Clumps

The detection of JCMT H_2D^+ is at a modest signal-to-noise (S/N) with five confirmed S/N peaks (5σ, 6σ, 7σ, 7σ, and 9σ) for a smoothed velocity resolution of ~ 0.2 km s^{-1}, therefore we obtained only source candidates. In Figure 1, the S/N map obtained (after baseline subtraction) is shown. To increase the S/N for the peak positions, we smoothed the original JCMT map using a symmetrical Gaussian point-spread function with a FWHM of two pixels, evaluated over a length of 10 pixels. Eighty percent of the pixels in the inner $90'' \times 90''$ of the map shown in Figure 1 have rms noise between 0.013 and 0.021 K. This resulted in our final map presented here with an FWHM beam of $19\farcs7$. The $>3\sigma$ detections in the S/N map were then confirmed by visualization of spectra in the smoothed map, and subsequent S/N analysis on Gaussian fits to the spectra. Similarly, three other $>3\sigma$ detections (also seen in Figure 1, for example, the contour between P4, P1, and P3)

[6] http://www.iram.fr/IRAMFR/GILDAS/

[7] The Submillimeter Array is a joint project between the Smithsonian Astrophysical Observatory and the Academia Sinica Institute of Astronomy and Astrophysics, and is funded by the Smithsonian Institution and the Academia Sinica.

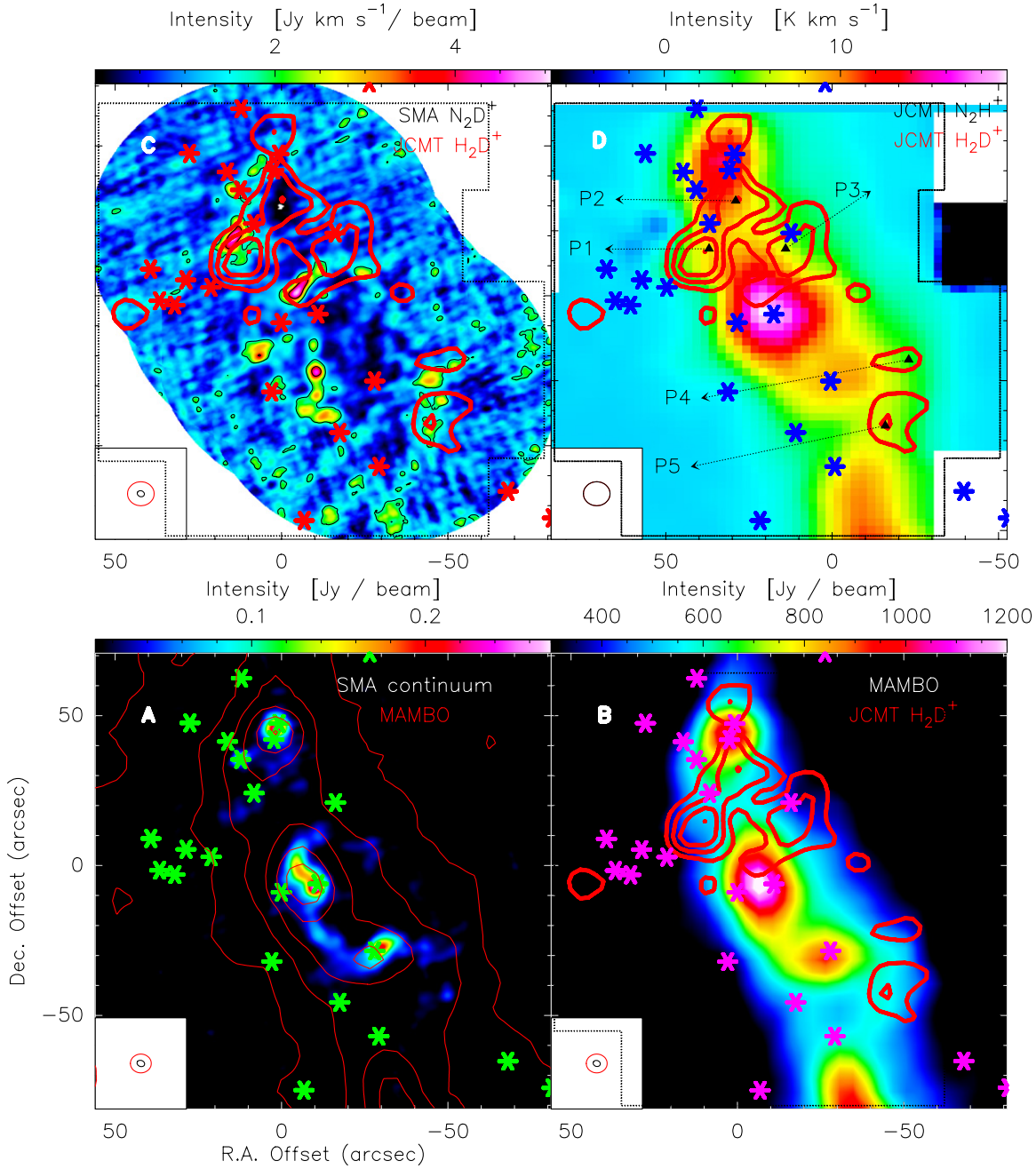

Figure 1. Panel (A, from left): SMA 1.3 mm dust continuum map which is a mosaic of four pointings (color scale) and MAMBO 1.3 mm map (contours, Motte et al. 2007). Panel (B): MAMBO 1.3 mm dust continuum and H_2D^+ S/N map as contours (contours, 3σ in steps of 1.5σ, where $0.013 \leqslant \sigma/\mathrm{K} \leqslant 0.021$). Panel (C): N_2D^+ 3–2 moment 0 map (weighted mean intensity integrated from -14 km s^{-1} to -8 km s^{-1}) and JCMT H_2D^+ S/N map (contours, 3σ in steps of 1.5σ). Panel (D): N_2H^+ 4–3 moment 0 map (weighted mean intensity integrated from -10 km s^{-1} to 3 km s^{-1}, gray scale) and JCMT H_2D^+ S/N map (contours, 3σ in steps of 1.5σ). The H_2D^+ core positions are marked as P"*n*". Stars denote the embedded population identified by Kumar et al. (2007).

(A color version of this figure is available in the online journal.)

were rejected by visualization of spectra. These might well be true detections, however, they require validation with deeper observations. Following these steps, we have confirmed five reliable detections (labeled P1 to P5) whose positional offsets and Gaussian fit parameters (obtained with CLASS) are tabulated in Table 2. The N_2H^+ (4–3) line parameters for data smoothed to the same spatial resolution are also given in the same table. The spectra toward the five positions for both lines are shown in Figure 2. The spectra have been converted from antenna temperature to main brightness temperature for a main beam efficiency of 0.63 (from the JCMT HARP Web page).

4.2. Spectral Line Features

The H_2D^+, N_2H^+, and N_2D^+ spectral line parameters toward the five H_2D^+ peaks are reported in Table 2. We also provide the non-thermal line width for these species after taking away the contribution due to thermal broadening at 15 K.

The H_2D^+ line toward even the brightest core (say P1) at offset (37″, 44″) is only modest at 0.18 K. Our brightest line is still fainter than the weakest H_2D^+ detection toward low-mass starless and prestellar cores reported so far (for a complete list, see Caselli et al. 2008). The LSR velocity toward the northern sources (P1, P2, P3) is systematically offset from

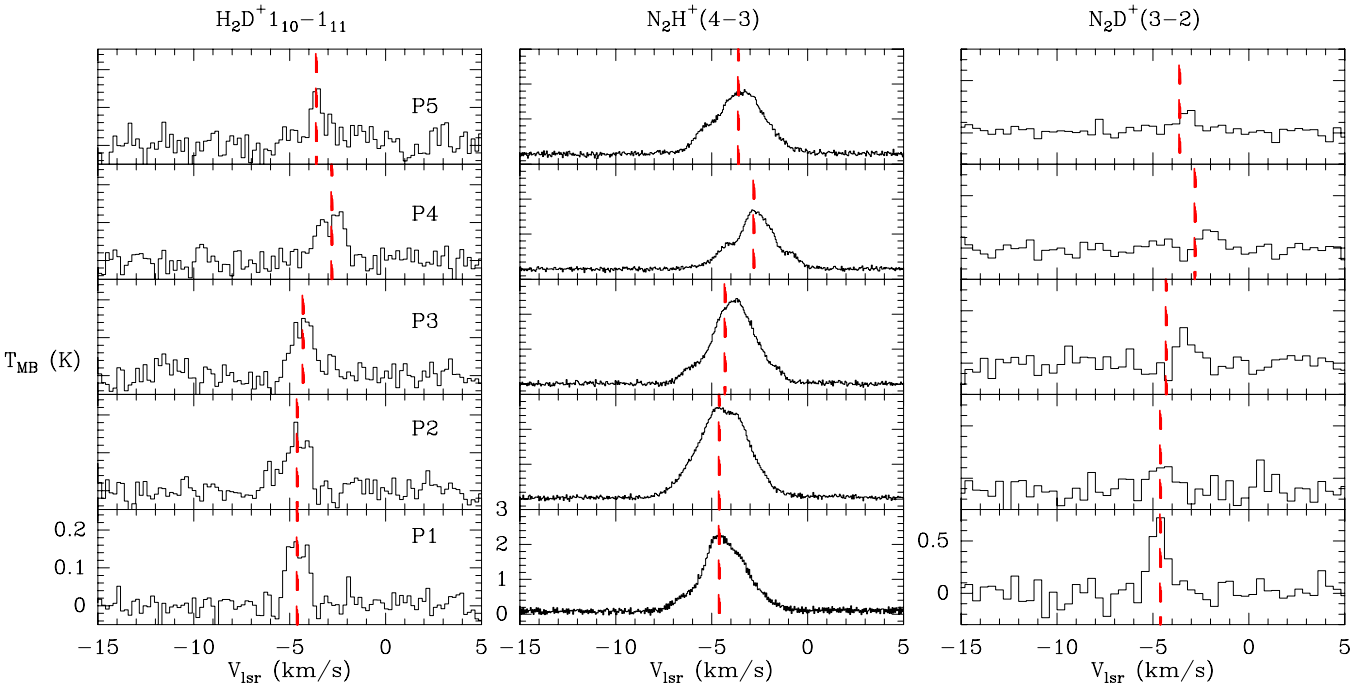

Figure 2. Left panel: JCMT spectra of H_2D^+ at 372.421 GHz. Centre panel: JCMT N_2H^+ 4–3 at 372.672 GHz. Right panel: SMA N_2D^+ 3–2 at 231.5 GHz. Spectra for all tracers have been extracted for the same spatial resolution, and the offset positions (in arcsecs) are as indicated in the figure. Note that the SMA spectra have a factor of two poorer spectral resolution than the JCMT spectra (∼0.2 km s^{-1}). H_2D^+ LSR velocity for each position is indicated as the line of reference in the three panels.

(A color version of this figure is available in the online journal.)

Table 2
Gaussian Fit Parameters from JCMT Observations

Source (R.A., Decl.) J2000	Molecule	T_{MB} (K)	V_{LSR} (km s^{-1})	Δv (km s^{-1})	Δv_{nt} (km s^{-1})	Velocity Range (km s^{-1})	$\int T_{MB}\, dv$ (K km s^{-1})
P1	H_2D^+ $1_{1,0}$–$1_{1,1}$	0.18 (0.02)	−4.6 (0.1)	1.20 (0.08)	1.13		
(20:39:03.7, +42:25:21)	N_2H^+ 4–3	3.27 (0.03)	−4.2 (0.1)	1.77 (0.02)	1.76	(−8.0,0.0)	9.65 (0.06)
	N_2D^+ 3–2	0.73 (0.14)	−4.8 (0.1)	0.82 (0.14)	0.81		
P2	H_2D^+ $1_{1,0}$–$1_{1,1}$	0.14 (0.02)	−4.6 (0.1)	1.50 (0.17)	1.44		
(20:39:03.1, +42:25:37)	N_2H^+ 4–3	4.15 (0.02)	−4.2 (0.1)	2.04 (0.01)	2.03	(−8.0,0.0)	13.72 (0.03)
	N_2D^+ 3–2	0.24 (0.12)	−4.7 (0.2)	0.85 (0.49)	0.84		
P3	H_2D^+ $1_{1,0}$–$1_{1,1}$	0.15 (0.02)	−4.3 (0.1)	1.26 (0.13)	1.19		
(20:39:01.7, +42:25:21)	N_2H^+ 4–3	3.69 (0.02)	−3.7 (0.1)	1.69 (0.16)	1.68	(−8.0,0.0)	10.79 (0.04)
	N_2D^+ 3–2	0.33 (0.13)	−3.5 (0.1)	0.67 (0.23)	0.65		
P4	H_2D^+ $1_{1,0}$–$1_{1,1}$	0.12 (0.02)	−2.8 (0.1)	1.61 (0.15)	1.56		
(20:38:58.3, +42:24:44)	N_2H^+ 4–3	2.40 (0.02)	−2.6 (0.1)	1.47 (0.01)	1.46	(−8.0,2.0)	6.93 (0.03)
	N_2D^+ 3–2	0.19 (0.07)	−2.2 (0.1)	0.69 (0.99)	0.67		
P5	H_2D^+ $1_{1,0}$–$1_{1,1}$	0.13 (0.07)	−3.6 (0.1)	0.82 (0.35)	0.71		
(20:38:58.9, +42:24:22)	N_2H^+ 4–3	2.77 (0.02)	−3.4 (0.1)	1.92 (0.01)	1.91	(−8.0,2.0)	9.30 (0.04)
	N_2D^+ 3–2	0.20 (0.08)	−3.3 (0.1)	0.74 (0.28)	0.72		

Notes. Δv and Δv_{nt} are the observed and non-thermal FWHM line width, respectively. Δv_{nt} is calculated after accounting for thermal line width at 15 K. Toward position P4, the H_2D^+ spectrum shows an asymmetry which if taken as due to two velocity components has line width (FWHM) of 0.88 and 0.68 km s^{-1} at LSR velocity of −3.3 and −2.4 km s^{-1}, respectively. The FWHM derived for H_2D^+ is from a simple Gaussian fit while that for N_2D^+ and N_2H^+ is from a hyperfine fit.

those of the southern cores (P4, P5). We find a range in line widths of $0.8 < \Delta v/\,\mathrm{km\,s^{-1}} < 1.6$. The thermal line width (FWHM) at 15 K is 0.4 km s^{-1}. Clearly, the line width has a significant non-thermal component as expected in such protocluster environments (also given in Table 2). Though it is difficult to assess the line profiles at the given S/N, a double-peaked profile is observed toward P4. The line asymmetry might be due to different velocity components along the line of sight, absorption in the core envelope or infall motions (as argued by van der Tak et al. 2005 where a similar H_2D^+ profile is observed in L1544). Clearly, high spatial resolution observations are required to clarify this.

The 4–3 line of N_2H^+ line is very bright (>2 K) and broad (⩾1.5 km s^{-1}) toward all the five offset positions. This transition has over 40 hyperfine lines within <5 km s^{-1}. The N_2D^+ 3–2 transition also has hyperfine structure (hfs) spread over 7 km s^{-1}. However, this is below our detection limit for all H_2D^+ peaks. Also, the S/N for N_2D^+ spectra toward H_2D^+ peaks is poor. Therefore, we refrain from any interpretation of the N_2D^+ spectra. H_2D^+ is much lighter than N_2D^+ and N_2H^+ (factor of seven) and hence the thermal line broadening is significant. The thermal line width (FWHM) at 15 K is 0.41 km s^{-1} for H_2D^+, much larger than 0.15 km s^{-1} for N_2H^+ and N_2D^+. However, in Cygnus X, the non-thermal contribution is still dominant. As

listed in Table 2, the intrinsic (i.e., taking the hfs structure into account) line widths of three species are different. Excluding P4 (where the N_2H^+ and H_2D^+ line widths are equal), H_2D^+ line width is lower than that of N_2H^+ and might imply that deuterated molecules preferably trace quiescent gas. The mean difference in line width for the H_2D^+–N_2H^+pair is 0.52(±0.48), i.e., the higher N_2H^+ line width with respect to H_2D^+ is only marginally significant.

The N_2H^+ LSR velocity is consistently red shifted relative to that of H_2D^+ and magnitude of this shift varies from 0.2 to 0.6 km s^{-1}.

4.3. H_2D^+, N_2D^+, N_2H^+, and Thermal Dust Continuum

The dust continuum emission at high (1.3 mm SMA, ∼ 3.″8) and coarser (1.3 mm MAMBO, ∼ 11″) angular resolution is shown in panels (A) and (B) of Figure 1. The MAMBO clumps fragment further with significant structure all along the filament. The subsequent panels in the figure show the gas distribution in three different tracers: H_2D^+, N_2D^+, and N_2H^+. There is very good correlation between thermal dust continuum and N_2H^+ emission with the brightest N_2H^+ emission coinciding with the bright MAMBO peaks (panel (D)). However, there is no such one-to-one correlation of dust continuum with either N_2D^+ (panel (C)) or H_2D^+ emission (panels (B)–(D)).

H_2D^+ is concentrated in five clumps distributed around the massive protocluster (panel (B), Figure 1). However, no H_2D^+ emission is seen toward any of the bright and dense dust cores seen with MAMBO/SMA. Conversely, no compact continuum is detected for H_2D^+ cores. The H_2D^+ distribution coincides with our SMA N_2D^+ 3–2 observations, however their peaks do not. Instead the N_2D^+ cores are distributed in further clumpy structures offset and partially surrounding the H_2D^+ peaks. Furthermore, there is one H_2D^+ peak (P1) with no associated N_2D^+ emission, and several N_2D^+ cores with no corresponding H_2D^+ emission. As seen in the fourth panel of Figure 1, there is always extended N_2H^+ emission associated with H_2D^+ cores.

4.4. ortho-H_2D^+ and N_2H^+ Abundance

The *ortho*-H_2D^+ column density for the different cores have been estimated following Vastel et al. (2006) from the main beam brightness temperature, line width, and assuming an excitation temperature (T_{EX}) of 10 K. The H_2D^+ line is optically thin in all cores (≪1) and the assumed T_{EX} also enters the optical depth estimation following Equation (4) of Vastel et al. (2006). Therefore, we note that the derived H_2D^+ column density crucially depends on the assumption of excitation temperature. A 30% decrease in T_{EX} lower than 10 K is poorly justified. Pillai et al. (2007) estimate an ammonia rotational temperature of 18 K in the vicinity of P4 (within 40″). The presence of H_2D^+ emission together with the lack of 24 μm emission toward the H_2D^+ cores rules out much higher gas temperatures (≫20 K). In their H_2D^+ sample of prestellar and protostellar cores, Caselli et al. find on average 3 K higher kinetic temperatures and higher T_{EX} for their protostellar cores as their prestellar cores (8 K versus 11 K). Friesen et al. (2010) also find a higher (than prestellar cores) T_{EX} of 12 K to be appropriate for their low-mass cluster-forming core in Ophiucus.

MAMBO 1.3 mm data smoothed to the resolution of the final JCMT data have been used to determine H_2 column density for a 15 K kinetic temperature following Kauffmann et al. (2008). We have used a dust opacity of 0.0102 cm^2 g^{-1} for dust grains with thin ice mantles and gas density $n(H) = 10^6$ cm^{-3} as in Ossenkopf & Henning (1994). The *ortho*-H_2D^+ column density and the resulting H_2D^+ abundances are reported in Table 3. The ratio between column density toward cores studied here and those observed toward low-mass cores (summarized in Table 3 of Caselli et al. 2008) varies from 1 to 13.

Table 3
H_2D^+, N_2H^+ Column Density and Abundance

Position	N(*o*-H_2D^+)[a] ($\times10^{12}$) cm^{-2}	$\chi_{o\text{-}H_2D^+}$[b] ($\times10^{-11}$)	$N(N_2H^+)$[c] ($\times10^{15}$) cm^{-2}	$\chi_{N_2H^+}$[d] ($\times10^{-8}$)
P1	3.8 (0.5)	1.9	2.0 (0.01)	1.0
P2	3.7 (0.7)	1.4	2.8 (0.01)	1.1
P3	3.3 (0.6)	1.7	2.2 (0.01)	1.1
P4	3.4 (0.7)	2.1	1.4 (0.01)	0.9
P5	1.9 (1.3)	0.9	1.9 (0.01)	0.9

Notes.
[a] The column density determined for excitation temperature, $T_{EX} = 10$ K.
[b] Fractional *ortho*-H_2D^+ abundance based on H_2 column density derived from MAMBO 1.3 mm data for dust temperature, $T_{KIN} = 15$ K.
[c] The N_2H^+ column density determined for excitation temperatures, $T_{EX} = 5$ K.
[d] Fractional N_2H^+ abundance based on H_2 column density derived from MAMBO 1.3 mm data for dust temperature, $T_{KIN} = 15$ K.

As mentioned before, the N_2H^+ hfs contributes significantly to the broadening of the line. We fit the N_2H^+ hyperfines (METHOD HFS in CLASS), and FWHM so obtained is much lower than from a GAUSS fit (Table 2; Gerin et al. 2001). The optical depth, and therefore the excitation temperature which is usually otherwise derived based on optical depth and line brightness is uncertain. Hence, the choice of excitation temperature is somewhat arbitrary and is based on observations in literature. For example, Fontani et al. (2008) derive excitation temperature close to 6 K value toward N_2H^+ cores in a high-mass star-forming region. Assuming optically thin condition, we have estimated the column density from the integrated intensity of N_2H^+ 4–3 lines following Caselli et al. (2002c) for an excitation temperature of 5 K. The total N_2H^+ abundance is tabulated in Table 3. The uncertainties given in brackets are formal errors obtained by a Gaussian error propagation.

5. DISCUSSION

While some of the results discussed above are intuitively easy to understand, many are not. In this section, we attempt to explain these anomalies and thus characterize the physical conditions.

The bright MAMBO sources are actively forming stars and clusters (Kumar et al. 2007), as also evidenced by their mid-infrared (mid-IR) emission. Higher temperatures and subsequent release of heavy neutrals (CO) from grain mantles destroy H_2D^+ and therefore reduce the deuterium reservoir in such bright cores. For example, from NH_2D observations we find clear evidence of the peak being offsets from the bright cores showing star formation activity (Pillai et al. 2011). The colder secondary cores, on the other hand, are expected to have abundant deuterated species. Are these secondary cores principally seen in H_2D^+ emission representative of the prestellar/cluster gas?

5.1. Extent of H_2D^+ Emission

The most surprising element of our observation is the widespread emission of H_2D^+ with no direct counterpart in previous dust continuum or line measurements (continuum data from Motte et al. 2007 and line data from Csengeri et al. 2011).

The H_2D^+ emission is instead distributed in cores around the bright continuum cores over a ~1pc region. The individual cores have an average diameter of 0.2 pc roughly estimated by fitting ellipses by eye (34,000 AU, P4 and P5 are smaller). This is more than twice the extent of H_2D^+ emission observed toward the only two regions previously mapped in H_2D^+; the low-mass prestellar core in Taurus (L1544; Vastel et al. 2006) and the low-mass cluster-forming core in Ophiucus (OphB2; Friesen et al. 2010).

In the past, H_2D^+ was thought to trace the innermost regions (few 1000 AU) of a dense core where all the heavier molecules deplete onto grain mantles with density exceeding 10^6 cm^{-3} (di Francesco et al. 2007). However, with newer data on the collisional rate of H_2D^+ the critical density of the transition has been corrected to $\sim 10^5$ cm^{-3}, an order of magnitude lower than previously assumed (Caselli et al. 2008). Combined with the prevalent cold temperature in such dense cores, this implies that the H_2D^+ distribution is expected to be much larger ($\gg$7000 AU). The extent of H_2D^+ distribution in OphB2 or L1544 can then be comprehended. However, it is surprising that in Cyg X this distribution is twice as large. Mapping of the entire DR21 filament is likely to discover more such cold quiescent gas pockets in an otherwise active high-mass star-forming region.

5.2. Absence of Dust Continuum Peaks Toward ortho-H_2D^+ Peaks

Although there is weaker dust emission toward all H_2D^+ cores, none of the H_2D^+ peaks have been detected as a peak in dust continuum emission with MAMBO as well as SMA. Depletion is often invoked to explain such lack of correlation between dust and gas in different tracers. However, the molecule in question is H_2D^+, one of the lightest deuterated ions that should survive depletion. Therefore, we suggest that dust continuum observation is partially misleading, i.e., not tracing mass distribution. We assert this by showing that H_2D^+ emission comes from a region of low temperature and high density.

We draw out the density in three different ways. First, let us define a spherical core around an H_2D^+ core, for example, P1. It has a mass of 137 $M_\odot$ within a radius of ~0.1 pc from MAMBO observations for a temperature of 15 K. This implies an average density of 5×10^6 cm^{-3}. Second, we extract the intensity of the filament in dust emission toward an intensity minima in between two bright MAMBO cores, considerably offset from the H_2D^+ cores and outside its 3σ boundary. Adopting the distance to the extreme ends of two H_2D^+ cores' boundary as a measure of the size of a typical core, in this case 60 arcsec, we again derive density (2×10^5 cm^{-3}). The critical density of the observed H_2D^+ transition at 20 K is $\sim 1.1 \times 10^5$ cm^{-3}. This shows that the density in a region larger than the H_2D^+ core by a factor of $\sim 60/20 = 3$ (20 arcsec corresponds to representative H_2D^+ core size) is still high enough to get H_2D^+ excited. Finally, N_2H^+ 4–3 emission is observed all along the filament including toward H_2D^+ cores. The critical density[8] of this N_2H^+ transition at 3×10^7 cm^{-3} is two orders of magnitude higher than that of the H_2D^+ transition, requiring very dense gas. Clearly not every region (like the envelope) in the filament can have such high densities or the implied high excitation temperature, and the line is likely sub-thermally excited (Evans 1999). We therefore used the non-LTE radiative transfer code RADEX[9] for a simple calculation of the expected N_2H^+ 4–3 line brightness for a column density of 10^{15} cm^{-2} and line width (FWHM) of 2 km s^{-1} at 20 K for a wide range of densities (guided by N_2H^+ line parameters for the H_2D^+ cores given in Tables 2 and 3). We are thus able to rule out densities below 10^5 cm^{-3} for the H_2D^+ cores.

Next, we look at the maximum temperature of the H_2D^+-emitting region. H_2D^+ cores are mid-IR-quiet at 24 μm, while the bright MAMBO cores have bright 24 μm point like emission as observed with the MIPS instrument on the *Spitzer* telescope (Spitzer Legacy Program ID 40184, PI: J. Hora), consistent with the notion that these bright objects are massive protostars (Chandler et al. 1993). A precise luminosity of these protostars is difficult to measure because the sources are saturated. Based on a single temperature spectral energy distribution (SED) fit to their far-infrared (FIR) and 1.3 mm data, Chandler et al. have determined the luminosity of one of the protostars in the region (known as FIR1) to be ~1860 $L_\odot$ (this value has been corrected for our adopted distance of 1.7 kpc instead of 3 kpc). Given the poor spatial resolution of the *IRAS* data, the individual protostars would in any case not be distinguished. We find two sources from the Red *Midcourse Space Experiment* (*MSX*) Source (RMS) survey of a large sample of massive young stellar objects from the *MSX* point-source catalog in our field (Hoare et al. 2005; Urquhart et al. 2008). The survey database at www.ast.leeds.ac.uk/RMS characterizes the luminosity of the two sources, G081.7522+00.5906, G081.7624+00.5916 as 2500 and 1000 $L_\odot$, respectively (Mottram et al. 2011). Assuming that FIR1/2/3 are in similar stages of evolution, we adopt 1000 $L_\odot$ as a conservative estimate of the protostellar luminosity. The mass-weighted dust temperature within an aperture of radius R is approximated using Equation (8) of Kauffmann et al. (2008). That equation assumes a simplified dust temperature dependence on radius and luminosity (i.e., calibrated by Terebey et al. 1993; $T_d \propto L^{0.2}/r^{0.4}$), but further requires temperatures $\geqslant$10 K. Assuming a density profile $\varrho \propto r^{-2}$, these temperatures are then weighed by mass to obtain the mean temperature (e.g., Belloche et al. 2006). Following Equations (5) and (8) from Kauffmann et al. (2008), the temperature at a radius of 30,000 AU (~17″) from the protostar would drop to 15 K. Here, the exact value of the radius is not relevant but within reasonable distance of the protostar the dust should be cold, a requisite for H_2D^+ emission.

So far we have shown that high density and low temperature—a necessary condition for H_2D^+ excitation—is satisfied in an extended region around the protostars. Therefore, the cores seen in H_2D^+ need not necessarily correspond to a 3D maximum in density. To the extent of the validity of our first-order calculations here in terms of effect or protostellar luminosity on heating, it is not required to have a density peak toward the H_2D^+ peaks. If we were to do more elaborate calculations to derive the density structure, then a density peak would have enhanced the cooling within the peak. However, the H_2D^+ peaks might well correspond to a temperature minima. We intend to investigate this via NH_3 measurements.

Why are the H_2D^+ cores not detected in SMA 1.3 mm dust continuum? The SMA continuum distribution is offset from the H_2D^+ peaks. Recall, however, that the H_2D^+ peaks need not be density peaks. Therefore, the fact that the dust peaks are offset is not inconsistent with the H_2D^+ observations. Even so, it is worth noting that all H_2D^+ cores are widely associated with SMA dust continuum peaks, i.e., offset from rather than being anti-correlated with continuum peaks. Based on the 1.3 mm MAMBO data, we calculated the total mass of the H_2D^+ cores.

[8] Derived based on N_2H^+ collisional rate from LAMDA database for a temperature of 20 K (Schöier et al. 2005).
[9] van der Tak et al. (2007).

We derive the gas mass at 15 K from the 1.3 mm following Kauffmann et al. (2008), using dust opacities at 1.3 mm (0.0102 $cm^2 g^{-1}$) for dust grains with thin ice mantles and gas density $n(H) = 10^6$ cm^{-3} as in Ossenkopf & Henning (1994), and gas to dust ratio of 100. The mass estimate is uncertain by a factor of two mainly due to the uncertain dust opacity. The typical mass of an H_2D^+ core is $\sim$130 $M_\odot$. However, we find that $\leqslant$10% mass resides in the cores detected with SMA. The missing matter might be either dense but smooth structures filtered out by an interferometer like the SMA. This is validated by our N_2D^+ SMA data. It is contaminated by negative bowls (see the third panel of Figure 1). This unwanted feature of synthesis array observations is a signature left by very extended objects that dominate the short spacings in the uv plane. Alternatively, a cluster of low-mass cores well below the sensitivity limit of the array would also explain the missing matter.

Given that 90% of the dust emission is missing in the SMA data, the lack of a one-to-one correlation between SMA continuum and H_2D^+ might not be significant. For example, consider the dust emission associated with clump P1. We know that $\sim$90% of the dust emission is filtered out with SMA. If the structure is smooth, then this $\sim$90% emission could be randomly removed from any position in clump P1. Therefore, the remaining emission might also be located at a random position within P1. Moreover, the offset between SMA dust and H_2D^+ peaks is suggestive of density not being the only criteria to have H_2D^+ peaks where they are observed. If it would have been the case, then naturally the peak with the highest density would be least likely to filtered out by SMA. Therefore, we believe that the H_2D^+ peaks might be dominated by temperature effects. The dust might be significantly cooler than in the surroundings (and definitely cooler than at the bright dust continuum peaks, where protostars are embedded). A similar reasoning was proposed by Di Francesco et al. (2004), who found that interferometric observations of N_2H^+ actually betrayed the presence of a dense and cold starless core N6 in Oph A with no distinct peak observed in millimeter dust continuum observations.

We have derived the virial mass of the H_2D^+ cores following Bertoldi & McKee (1992). For a mean radius of 0.1 pc and FWHM $\Delta v = 1.2$ km s^{-1}, the virial mass of an H_2D^+ core is 30 $M_\odot$. The average virial mass is 28 $M_\odot$, very small compared to the mass derived from MAMBO observations. Therefore, these cores are gravitationally super-critical. The line width is highly supersonic (>1 km s^{-1}), for all but one core (P4). The high line width is another indication of a clumpy substructure within each H_2D^+ emitting region.

5.3. Absence of N_2D^+ Peaks toward ortho-H_2D^+ Peaks

As noted before, while N_2D^+ emission as observed at high angular resolution with SMA is widely associated with H_2D^+, the peaks of these two ions however do not coincide. Lack of N_2D^+ emission toward P2 is at least partially due to the problem of short spacing discussed in Section 5.2. Briefly, if the N_2D^+ emission is as extended as the observed H_2D^+ emission, then a significant fraction of this emission is likely to be filtered out by the SMA. We intend to pursue single-dish observations to address this issue. Two cases deserve more attention and are discussed here. First, N_2D^+ is seen to skirt the H_2D^+ emission in non-uniform clumpy structures except in the case of P2. The critical density for the 3–2 transitions of this line is an order of magnitude higher than our H_2D^+ transition. This implies that higher density is a requisite for its excitation. We have also shown that the H_2D^+ peaks at low resolution need not be density peaks. The SMA continuum cores, however, should point us toward the highest density compact cores in the vicinity of H_2D^+ emission. It is exactly here that N_2D^+ emission is concentrated.

Next, two of the N_2D^+ clumps in the southwest part of the region are devoid of H_2D^+ emission. It is difficult to understand why there are N_2D^+ cores with no H_2D^+ emission. Here, however, excitation might play a role. Also, given that the SMA data are prone to artifacts due to the uncertainties inherent in interferometric observations, these structures might be spurious. However, we downloaded published and archived $H^{13}CO^+$ 1–0 Plateau de Bure Interferometer taken at similar resolution to our SMA observations. The region is known as MDC N53 (Csengeri et al. 2011). Clearly, there is $H^{13}CO^+$ emission toward all the N_2D^+ features including the two features not detected in H_2D^+. The peak N_2D^+ and $H^{13}CO^+$ line brightness are however much weaker (more than a factor of four) toward these N_2D^+ cores. If the same scaling of line brightnesses is applied to H_2D^+, then it is evident why H_2D^+ is not detected (our highest H_2D^+ S/N is 8).

5.4. Depletion of N-bearing Molecules

We will now discuss the distribution of N_2H^+ and H_2D^+. At the low temperature of molecular clouds ($T < 20$ K), H_2D^+ is the primary ion for deuterium transfer to other molecules including N_2, which produces N_2D^+. Therefore, colder cores exhibit high deuteration as seen in the fractionation of molecules like N_2H^+, i.e., high $[N_2D^+]/[N_2H^+]$. However, at such low temperatures molecules freezeout onto dust grains. This not only includes CO and its derivatives like HCO^+ but also N-bearing molecules like N_2 (and consequently N_2H^+ and NH_3, which are both formed by molecular nitrogen). H_2D^+, on the other hand, can become abundant under such conditions where all heavy species have disappeared (depleted). To test this, we looked at the abundance distribution of N_2H^+ over the region. While the average N_2H^+ abundance of H_2D^+ cores is 1×10^{-8}, no significant variation from those position offset from H_2D^+ cores is found. The highest abundance is found toward the MAMBO bright peaks which are however higher by only a factor of $\sim$2. Given that our resolution is no finer than 34,000 AU, this result is not surprising. Stronger depletion might well be observed on much smaller spatial scales. While the estimated N_2H^+ abundance of $\sim 10^{-8}$ might seem significantly higher than that found in low-mass star-forming regions with typical abundance of $\sim 10^{-10}$ (Caselli et al. 2002a; Keto et al. 2004), we caution that the somewhat arbitrary choice of T_{EX} (5 K) influences this calculation. The higher column densities characteristic of high-mass star-forming regions might explain the high abundance, however a T_{EX} higher by 2 K is sufficient to lower the derived abundance by one order of magnitude.

5.5. Deuterium Chemistry

How does the observed *ortho*-H_2D^+ abundance compare to existing chemical models? Given the poor spatial resolution of our H_2D^+ observations, a tailored chemical model is not warranted. Qualitative comparisons can still be made with models that have focused on the H_2D^+ chemistry in dark clouds (Walmsley et al. 2004; Flower et al. 2004). To do this, we need to convert the observed *ortho*-H_2D^+ abundance to the total H_2D^+ abundance assuming an *ortho*-to-*para* (o/p) ratio for H_2D^+. Few observations have constrained this value in dark clouds ($\simeq$0.8 in L1544; Vastel et al. 2006). Assuming an o/p-H_2D^+ ratio as in L1544, we get a total H_2D^+ abundance

of $\sim 3 \times 10^{-11}$. However, if the gas temperature is even a few degrees warmer than in low-mass star-forming regions, then the o/p-H_2D^+ would drop, as shown in Figure 6 of Flower et al. (2004). This is mainly due to the dependence of o/p-H_2D^+ on o/p-H_2, and an increase in *ortho*-H_2 as shown by chemical models (Pagani et al. 1992). Such a drop in the *ortho*-H_2D^+ column density was already noticed by Caselli et al. (2008) toward warmer starless cores and protostellar cores in their sample with higher deuterium fractionation (R_D). We do not have temperature or R_D measurements toward all the H_2D^+ cores. However, Pillai et al. (2007) estimate a high rotational temperature of 18 K in the vicinity of P4 (within 40″) and $R_D = 0.34$, where R_D is measured as the ratio of NH_2D to NH_3 column density. This corresponds to an o/p-H_2D^+ ratio of about 0.6 (from Figure 6 of Flower et al. 2004). We also compared our *ortho*-H_2D^+ abundance to the dynamical model of Flower et al. (2006) that incorporates deuterium chemistry in the early stages of protostellar collapse, specifically their Figure 6 where *ortho*-H_2D^+ abundance at 10 K is plotted as a function of the gas density during collapse. For a density of $\sim 5 \times 10^5$ cm^{-3} o/p-H_2 close to 0.03 is consistent with our observations. An o/p-H_2 of $\ll 1$ that we indirectly infer is consistent with those measured in nearby low-mass star-forming regions. Observations of deuterated molecules with its parent molecule, for example, DCO^+/HCO^+ (Maret & Bergin 2007), $N_2D^+N_2H^+$ (Pagani et al. 2009), non-LTE radiative transfer modeling of H_2CO absorption (Troscompt et al. 2009), abundance ratio of nitrogen hydrides (Dislaire et al. 2012) have all delivered o/p-H_2 of $\ll 0.1$. This implies that the *para*-H_2 dominates in molecular clouds. Similar work in high-mass star-forming region is yet to be done. Detailed modeling should be made with higher resolution data together with tighter constraints on the density and temperature in Cygnus X.

5.6. H_2D^+ Emission in High- and Low-mass Star-forming Regions

We present here the first map of H_2D^+ distribution in a high-mass star-forming region. Previously, single spectra of H_2D^+ have been reported in at least two such regions, OriB9, a 100 $M_\odot$ cold, quiescent core in OrionB (Harju et al. 2006) and $\sim 4\sigma$ detection in a core in IRDC *MSX* G030.88+00.13 (Swift 2009). The *ortho*-H_2D^+ abundance in Cygnus X is in between the values for OriB9 ($\sim 10^{-10}$) and IRDCs $\sim 10^{-13}$. However, Cygnus X is also intermediate between these two regions in terms of its distance from us. Therefore, the extreme range in H_2D^+ abundance might merely reflect the effect of beam dilution. However, the line width of our H_2D^+ cores are similar to the core in G030.88+00.13 (0.9 km s^{-1}), and a factor of two higher than in OriB9 ($\sim$0.4 km s^{-1}). We also note that due to a lack of continuum data, Harju et al. derive OriB9 abundance based on the known ammonia abundance in the region (not toward the core), and might be offset from its true value. The H_2D^+ column density in OrionB9 itself is comparable to Cygnus X. The difference in line width is also reconciled if we account for the different spatial scales probed. Using the line width–size relation with an exponent of 0.4, if we were to scale the line width at a physical resolution of 0.03 pc, i.e., 17″ FWHM APEX beam at 410 pc to that at 0.16 pc (13″ FWHM JCMT beam at 1700 pc), the expected line width is even higher than the observed line width. Therefore, the physical conditions in Cygnus X might be similar to those in the quiescent and massive core in Orion.

As noted before, the average *ortho*-H_2D^+ abundance in Cygnus X is a factor of 1–20 lower than that in low-mass cores (Caselli et al. 2008). Assuming that the true abundance is similar to what is measured in low-mass star-forming regions, this might be due to a low filling factor. In that case H_2D^+ emission would be widespread but concentrated in small regions, with a filling factor of $\sim$0.1. H_2D^+ has been mapped in two low-mass star-forming regions, Oph B2, a dense core in the low-mass cluster-forming region in Ophiucus (Friesen et al. 2010), and L1544, a prestellar core in Taurus (Vastel et al. 2006). The peak H_2D^+ abundance in L1544 is an order of magnitude higher than for Cygnus X. Vastel et al. have used a spherically symmetric chemical model incorporating the physical structure of the cloud (density, temperature), and fit the abundance variation of H_2D^+ as a function of distance from the core center. While the best fit to their H_2D^+ finds a peak at 10^{-10}, $\chi_{o\text{-}H_2D^+}$ drops to $\sim 10^{-11}$ at $\sim$10,000 AU from the center, still smaller than our typical $\sim$17,000 AU radii. This re-affirms our earlier conclusion that these observations have uncovered extended cold dense gas that were undetected with typical molecular line and dust continuum surveys. Motte et al. (2007) surveyed the entire complex with MAMBO with the goal of identifying high-mass cores at the earliest stage of evolution, but did not find high-mass analogs of prestellar dense cores. In the region of overlap with our H_2D^+ map, a single object (CygX-N53) has been identified as a massive dense core, which is distinctly offset from the H_2D^+ cores. However, the three massive dense, colder (and younger) cores discovered by this work (P1, P2, P3) are also undetected in line observations ($H^{13}CO^+$ and HCN 1–0) of Csengeri et al. (2011).

Now, L1544 is a prestellar core with just enough mass (8 $M_\odot$; Tafalla et al. 1998) to form a single low-mass star. Oph B2, on the other hand, is a low-mass cluster-forming core. Many of the H_2D^+ line properties in Cygnus X are mirrored in Oph B2. Namely, the H_2D^+ peak is offset from the dust as well as N_2D^+ peaks. The line widths are higher than in L1544, although still transonic. The emission is also distributed over a larger region. H_2D^+ core sizes are not constrained by these observations, however the whole emission extends to $\sim$14,000 AU. Naively, the more extreme H_2D^+ properties in a high-mass region like Cygnus X seems to be scaled up from low-mass clusters.

6. SUMMARY

We present the first map of *ortho*-H_2D^+ $J_{k^+,k^-} = 1_{1,0} \rightarrow 1_{1,1}$ transition in a high-mass star-forming region. Distributed over a physical scale of 1 pc in at least five clumpy structures, this is also the largest H_2D^+ map of any star-forming region. The detection is weak and shows an anti-correlation with star formation, wherein H_2D^+ clearly avoids the active star-forming clusters, however, is still in their vicinity and has no IR emission of its own. The H_2D^+ emission is widely associated with dense dust emission as well as N_2D^+ as observed with SMA at high angular resolution. However, surprisingly the dust and N_2D^+ peaks are distinctly offset from the H_2D^+ peaks. While the derived H_2D^+ abundance is up to an order of magnitude lower than in low-mass star-forming regions, the N_2D^+ and N_2H^+ column density and abundance are comparable to or even higher than low-mass star-forming regions. The lack of local dust counterparts remains to be better understood. Our best reasoning is that H_2D^+ cores might have significantly clumpy substructure with temperature minima at the observed H_2D^+ peaks that need not be density peaks. We have thus shown that H_2D^+ is as good and unique a tool in tracing the cold and dense gas in

low-mass star-forming regions as in such complex massive star-forming regions. We have discovered a large reservoir of cold and dense gas undetected by previous surveys that were targeted at identifying the earliest stages of high-mass star formation. This suggests that the submillimeter continuum studies alone which are aimed at detecting massive prestellar cores might fail to identify a large population of such cores in earliest stages. Sensitive H_2D^+ mapping of the entire DR21 filament is likely to discover more of such cold quiescent gas reservoirs in an otherwise active high-mass star-forming region.

We are grateful to Dr. Iain Coulson and the JCMT staff for their kind support with observations and data handling. The James Clerk Maxwell Telescope is operated by The Joint Astronomy Centre on behalf of the Science and Technology Facilities Council of the United Kingdom, the Netherlands Organisation for Scientific Research, and the National Research Council of Canada. The JCMT data were obtained under the program ID M07BU14. This research was supported by an appointment of J.K. to the NASA Postdoctoral Program at the Jet Propulsion Laboratory, administered by Oak Ridge Associated Universities through a contract with NASA. It was executed at the Jet Propulsion Laboratory, California Institute of Technology, under contract with the National Aeronautics and Space Administration. T.P. acknowledges support from the Combined Array for Research in Millimeter-wave Astronomy (CARMA), which is supported by the National Science Foundation through grant AST 05-40399. T.P. acknowledges support from the SMA Fellowship Program while working on this project. A significant part of this work was done at the Center for Astrophysics, MA, USA.

Facilities: JCMT(HARP), SMA, Spitzer (IRAC)

REFERENCES

Bacmann, A., Lefloch, B., Ceccarelli, C., et al. 2003, ApJ, 585, L55
Belloche, A., Hennebelle, P., & André, P. 2006, A&A, 453, 145
Bertoldi, F., & McKee, C. F. 1992, ApJ, 395, 140
Beuther, H., Schilke, P., Menten, K. M., et al. 2002, ApJ, 566, 945
Bontemps, S., Motte, F., Csengeri, T., & Schneider, N. 2010, A&A, 524, A18
Caselli, P., Benson, P. J., Myers, P. C., & Tafalla, M. 2002a, ApJ, 572, 238
Caselli, P., van der Tak, F. F. S., Ceccarelli, C., & Bacmann, A. 2003, A&A, 403, L37
Caselli, P., Vastel, C., Ceccarelli, C., et al. 2008, A&A, 492, 703
Caselli, P., Walmsley, C. M., Zucconi, A., et al. 2002b, ApJ, 565, 331
Caselli, P., Walmsley, C. M., Zucconi, A., et al. 2002c, ApJ, 565, 344
Chandler, C. J., Gear, W. K., & Chini, R. 1993, MNRAS, 260, 337
Chen, H.-R., Liu, S.-Y., Su, Y.-N., & Zhang, Q. 2010, ApJ, 713, L50
Crapsi, A., Caselli, P., Walmsley, C. M., et al. 2004, A&A, 420, 957
Crapsi, A., Caselli, P., Walmsley, C. M., et al. 2005, ApJ, 619, 379
Csengeri, T., Bontemps, S., Schneider, N., Motte, F., & Dib, S. 2011, A&A, 527, A135
Di Francesco, J., André, P., & Myers, P. C. 2004, ApJ, 617, 425
di Francesco, J., Evans, N. J., II, Caselli, P., et al. 2007, in Protostars and Planets V, ed. B. Reipurth, D. Jewitt, & K. Keil (Tucson, AZ: Univ. Arizona Press), 17
Dislaire, V., Hily-Blant, P., Faure, A., et al. 2012, A&A, 537, A20
Evans, N. J., II 1999, ARA&A, 37, 311
Flower, D. R., Pineau des Forêts, G., & Walmsley, C. M. 2004, A&A, 427, 887
Flower, D. R., Pineau Des Forêts, G., & Walmsley, C. M. 2006, A&A, 449, 621
Fontani, F., Caselli, P., Bourke, T. L., Cesaroni, R., & Brand, J. 2008, A&A, 477, L45
Fontani, F., Palau, A., Caselli, P., et al. 2011, A&A, 529, L7
Friesen, R. K., Di Francesco, J., Myers, P. C., et al. 2010, ApJ, 718, 666
Gerin, M., Pearson, J. C., Roueff, E., Falgarone, E., & Phillips, T. G. 2001, ApJ, 551, L193
Harju, J., Haikala, L. K., Lehtinen, K., et al. 2006, A&A, 454, L55
Hoare, M. G., Lumsden, S. L., Oudmaijer, R. D., et al. 2005, in IAU Symp. 227, Massive Star Birth: A Crossroads of Astrophysics, ed. R. Cesaroni, M. Felli, E. Churchwell, & M. Walmsley (Cambridge: Cambridge Univ. Press), 370
Kauffmann, J., Bertoldi, F., Bourke, T. L., Evans, N. J., II, & Lee, C. W. 2008, A&A, 487, 993
Keto, E., Rybicki, G. B., Bergin, E. A., & Plume, R. 2004, ApJ, 613, 355
Kumar, M. S. N., Davis, C. J., Grave, J. M. C., Ferreira, B., & Froebrich, D. 2007, MNRAS, 374, 54
Maret, S., & Bergin, E. A. 2007, ApJ, 664, 956
Miettinen, O., Hennemann, M., & Linz, H. 2011, A&A, 534, A134
Motte, F., Bontemps, S., Schilke, P., et al. 2007, A&A, 476, 1243
Mottram, J. C., Hoare, M. G., Urquhart, J. S., et al. 2011, A&A, 525, A149
Ossenkopf, V., & Henning, T. 1994, A&A, 291, 943
Pagani, L., Salez, M., & Wannier, P. G. 1992, A&A, 258, 479
Pagani, L., Vastel, C., Hugo, E., et al. 2009, A&A, 494, 623
Pillai, T., Kauffmann, J., Wyrowski, F., et al. 2011, A&A, 530, A118
Pillai, T., Wyrowski, F., Hatchell, J., Gibb, A. G., & Thompson, M. A. 2007, A&A, 467, 207
Roberts, H., Herbst, E., & Millar, T. J. 2004, A&A, 424, 905
Sakai, T., Sakai, N., Furuya, K., et al. 2012, ApJ, 747, 140
Schöier, F. L., van der Tak, F. F. S., van Dishoeck, E. F., & Black, J. H. 2005, A&A, 432, 369
Shu, F. H., Adams, F. C., & Lizano, S. 1987, ARA&A, 25, 23
Sridharan, T. K., Beuther, H., Schilke, P., Menten, K. M., & Wyrowski, F. 2002, ApJ, 566, 931
Swift, J. J. 2009, ApJ, 705, 1456
Tafalla, M., Mardones, D., Myers, P. C., et al. 1998, ApJ, 504, 900
Terebey, S., Chandler, C. J., & Andre, P. 1993, ApJ, 414, 759
Thompson, M. A., Gibb, A. G., Hatchell, J. H., Wyrowski, F., & Pillai, T. 2005, in The Dusty and Molecular Universe: A Prelude to Herschel and ALMA, ed. A. Wilson (Noordwijk: ESA), 425
Troscompt, N., Faure, A., Maret, S., et al. 2009, A&A, 506, 1243
Urquhart, J. S., Hoare, M. G., Lumsden, S. L., Oudmaijer, R. D., & Moore, T. J. T. 2008, in ASP Conf. Ser. 387, Massive Star Formation: Observations Confront Theory, ed. H. Beuther, H. Linz, & T. Henning (San Francisco, CA: ASP), 381
van der Tak, F. F. S., Black, J. H., Schöier, F. L., Jansen, D. J., & van Dishoeck, E. F. 2007, A&A, 468, 627
van der Tak, F. F. S., Caselli, P., & Ceccarelli, C. 2005, A&A, 439, 195
Vastel, C., Caselli, P., Ceccarelli, C., et al. 2006, ApJ, 645, 1198
Walmsley, C. M., Flower, D. R., & Pineau des Forêts, G. 2004, A&A, 418, 1035